Polym. Korea, Vol. 50, No. 2, pp. 340-347 (2026) ISSN 2234-8077(Online)
https://doi.org/10.7317/pk.2026.50.2.340

Benzo[1,2,5]thiadiazole 기반 비융합형 비풀러렌 단분자 전자 수용체의 플루오린화가 고분자 태양전지 성능에 미치는 영향

박경헌*,# · 송창은**,***,# · 피자 아르샤드**,*** · 임은희*,†
*서울시립대학교 융합응용화학과, **한국화학연구원, ***과학기술연합대학원대학교
(2025년 11월 24일 접수, 2026년 1월 14일 수정, 2026년 1월 27일 채택)

Effect of Fluorination of Benzo[1,2,5]thiadiazole-Based Nonfused Nonfullerene Small Molecular Acceptors on Polymer Solar Cell Performance

Kyoungheon Park*,#, Chang Eun Song,***,#, Fiza Arshad**,***, and Eunhee Lim*,†**
**Department of Applied Chemistry, University of Seoul, 163 Seoulsiripdae-ro, Dongdaemun-gu, Seoul 02504, Korea*
***Korea Research Institute of Chemical Technology (KRICT), 141 Gajeongro, Yuseong-gu, Daejeon 34114, Korea*
****Advanced Materials and Chemical Engineering, University of Science and Technology (UST), Daejeon 34113, Korea*
(Received November 24, 2025; Revised January 14, 2026; Accepted January 27, 2026)

초록: 우리는 고분자 도너와 혼합하여 고분자 태양전지의 활성층으로 활용하기 위해, 막대 모양의 비풀러렌 단분자 어셉터 시리즈인 T-BT-T-ORH, T-1FBT-T-ORH, T-2FBT-T-ORH를 개발하였다. 이들 비풀러렌 단분자 어셉터들은 간단한 티오펜–벤조[1,2,5]티아디아졸(BT)–티오펜(T-BT-T) 중심 구조에 옥틸 치환 로다닌을 말단기로 도입한 형태를 가지며, BT 그룹에 0, 1, 또는 2개의 플루오린 원자를 도입함으로써 그 특성을 체계적으로 조절하였다. 이러한 플루오린화 전략은 전자 끌림 강도를 정밀하게 제어할 수 있게 하였으며, 구조 변화와 에너지 준위 정렬, 응집 거동, 그리고 소자 성능 간의 상관관계를 명확히 규명할 수 있는 틀을 마련하였다. 플루오린화된 분자들은 향상된 분자 결정성과 안정화된 경계 궤도 준위를 나타낸 반면, 비플루오린화된 T-BT-T-ORH는 우수한 용해도와 박막 모포로지를 보여 더 높은 소자 효율을 달성하였다. 세 NFSM 모두 poly[4,8-bis[5-(2-ethylhexyl)thiophen-2-yl]benzo[1,2-b:4,5-b']-dithiophene-2,6-diyl-alt-3-fluoro-2-[(2-ethylhexyl)carbonyl]-thieno[3,4-b]thiophene-4,6-diyl] (PTB7-Th) 고분자 도너와 함께 고분자 태양전지의 어셉터로 사용되었으며, 플루오린화 정도에 따라 성능이 달라졌다. 본 연구는 비풀러렌 단분자 어셉터 설계에서 플루오린화의 가능성과 한계를 동시에 보여주며, 고성능 고분자 태양전지 구현에 필요한 균형 잡힌 전자적 특성과 바람직한 박막 형태를 달성하기 위해 정밀한 치환 전략이 중요함을 보여준다.

Abstract: We developed rod-shaped non-fullerene small molecule (NFSM) acceptors, **T-BT-T-ORH**, **T-1FBT-T-ORH**, and **T-2FBT-T-ORH**, designed for blending with polymer donors for use as the active layer in polymer solar cells (PSCs). These NFSMs feature a simple thiophene–BT–thiophene (T-BT-T) core end-capped with octyl-substituted rhodanines (RHs), and their properties were systematically tuned by introducing 0, 1, or 2 fluorine atoms into the benzo[1,2,5]thiadiazole (BT) units. Such systematic fluorination of the BT unit enables the controlled modulation of the electron-withdrawing strength, establishing a clear framework to correlate structural changes with energy-level alignment, aggregation behavior, and device performance. The fluorinated molecules exhibited enhanced molecular crystallinity and stabilized frontier orbital levels, whereas the non-fluorinated **T-BT-T-ORH** showed superior solubility and film morphology, leading to higher device efficiency. All three NFSMs functioned as acceptors in polymer solar cells (PSCs) with a poly[4,8-bis[5-(2-ethylhexyl)thiophen-2-yl]benzo[1,2-*b*:4,5-*b*']-dithiophene-2,6-diyl-*alt*-3-fluoro-2-[(2-ethylhexyl)carbonyl]-thieno[3,4-*b*]thiophene-4,6-diyl] (PTB7-Th) polymer donor, and their performance was strongly influenced by the extent of fluorination. These findings revealed both the opportunities and limitations of fluorination in NFSM design, demonstrating the importance of precise substitution strategies for achieving balanced electronic properties and favorable film morphologies in high-performance PSCs.

Keywords: benzo[1,2,5]thiadiazole, fluorination, polymer solar cell, acceptor.

#K. Park and C. E. Song contributed equally to this work.
†To whom correspondence should be addressed.
ehlim@uos.ac.kr, ORCID 0000-0002-2321-7072

Introduction

Polymer solar cells (PSCs) are considered one of the promising candidates in photovoltaic technology owing to their low material cost, mechanical flexibility, light weight, and optical transparency.[1-8] In particular, rapid advances in PSCs, enabled by polymer donors in combination with fused-ring non-fullerene small molecule (NFSM) acceptors such as ITIC[9] and Y6,[10] have pushed the power conversion efficiencies (PCEs) exceeding 20%.[11-14] These achievements are attributed to the effective control of the electron-donating and electron-accepting units within the molecular backbones of the donors and acceptors, underscoring that precise molecular structural engineering is essential for optimizing device performance.[15] In addition to fused-ring NFSMs, non-fused-ring acceptors that have been engineered to address key limitations such as molecular planarity and charge transport have demonstrated competitive efficiencies exceeding 18%, highlighting their potential as cost-effective and synthetically accessible alternatives.[16,17]

Benzo[1,2,5]thiadiazole (BT) is a representative electron-deficient building block, employed in π-conjugated small molecules and polymers owing to its highelectron-withdrawing ability and structural tunability.[18] Various substituents have been introduced onto the BT-ring, including electron-withdrawing groups such as halogen atoms, electron-donating groups such as alkoxy moieties, and heteroatom variants such as pyridal[1,2,5]thiadiazole. Such modifications enable the precise modulation of frontier orbital energies, intermolecular interactions, and solid-state packing, thereby influencing charge transport and device efficiency[19-22] Fluorination effectively stabilizes frontier orbital levels, reinforces noncovalent interactions (e.g., F–S, F–H) and modulates dipole moments with minimal steric hinderance.[23,24] Modulating the number of fluorine atoms on the BT core provides a clear relationship between electron-withdrawing strength, energy-level alignment, aggregation/packing behavior, and device efficiency. Chen *et al*. reported the fluorination of Y-type NFSMs, in which the incorporation of fluorine atoms widened the band gap and promoted stronger molecular aggregation. These structural modifications enhance intermolecular packing and charge transport, ultimately yielding PSCs with PCEs exceeding 18%.[25]

In the present work, we developed a series of BT-rhodanine (RH)-based small molecules to systematically investigate the effect of fluorine substitution (0, 1, and 2 F atoms in BT) within a structurally identical rod-shaped NFSM backbone. All three A–D–A–D–A-type small molecules, **T-BT-T-ORH**, **T-1FBT-T-ORH**, and **T-2FBT-T-ORH**, consist of a thiophene-BT-thiophene (T-BT-T) core and octyl-substituted RH (ORH) terminal units. The T-BT-T core in **T-BT-T-ORH** was modified to contain a single F atom or two F atoms on the BT, resulting in **T-1FBT-T-ORH** and **T-2FBT-T-ORH**. Their physical properties, including frontier energy levels and packing behaviors, were systematically studied using differential scanning calorimetry (DSC), UV-vis absorption, and cyclic voltammetry (CV) measurements. Finally, PSC devices were constructed employing these molecules as acceptors and poly[4,8-bis(5-(2-ethylhexyl) thiophen-2-yl)benzo[1,2-b;4,5-b']dithiophene-2,6-diyl-alt-(4-(2-ethylhexyl)-3-fluorothieno[3,4-b]thiophene-)-2-carboxylate-2-6-diyl)](PTB7-Th) as the polymer donor.

Experimental

Synthesis. Synthesis of **T-BT-T-ORH**: B-T-ORH (600 mg, 1.29 mmol), 4,7-dibromobenzo[*c*]-1,2,5-thiadiazole (172 mg, 0.586 mmol), and tri-*tert*-butylphosphonium tetrafluoroborate ($P(t\text{-}Bu)_3 \cdot HBF_4$, 10.4 mg) were dissolved in distilled tetrahydrofuran (30 mL). Aqueous 1 M potassium phosphate tribasic (K_3PO_4, 1.70 mL) was then added, followed by tris(dibenzylideneacetone)dipalladium(0) ($Pd_2(dba)_3$, 16.0 mg). After degassing, the mixture was refluxed and stirred for 8.5 h under a nitrogen atmosphere. The reaction mixture was then extracted with dichloromethane, washed with water, and dried over $MgSO_4$. The crude product was purified using column chromatography (dichloromethane) to afford **T-BT-T-ORH** as a red solid (302 mg, 63% yield). ^{1}H NMR (400 MHz, $CDCl_3$), δ (ppm): 8.38 (*d*, *J* = 4.2 Hz, 1H), 7.93 (*s*, 1H), 7.59–7.50 (*m*, 1H), 4.19–4.06 (*m*, 2H), 1.73 (*s*, 2H), 1.30 (*t*, *J*=20.5 Hz, 10H), 0.89 (*t*, *J*=6.9 Hz, 3H). ^{13}C NMR (126 MHz, tetrachloroethane), δ (ppm): 195.34, 170.41, 155.20, 149.34, 142.72, 137.85, 132.20, 129.10, 128.93, 127.92, 124.95, 48.08, 34.81, 32.17, 32.14, 30.06, 29.86, 25.67, 17.16. Anal. Calcd. For $C_{38}H_{42}N_4O_2S_7$: C, 56.26; H, 5.22; N, 6.91; S, 27.67. Found: C, 56.58; H, 5.12; N, 6.80; S, 27.92.

Synthesis of **T-1FBT-T-ORH**: The synthetic procedure was performed under conditions analogous to those used for **T-BT-T-ORH**. 4,7-Diiodo-5-fluorobenzo[c][1,2,5]thiadiazole (240 mg, 0.60 mmol) and B-T-ORH (700 mg, 1.50 mmol) were used as starting materials, together with $Pd_2(dba)_3$ (16.0 mg), $P(t\text{-}Bu)_3 \cdot HBF_4$ (10.0 mg), and THF (20 mL)/1 M K_3PO_4 (1.6 mL). After refluxing for 8.5 h under a nitrogen atmosphere, the product was purified using column chromatography to afford **T-1FBT-T-ORH** as a purple solid (448 mg, 90% yield). ^{1}H NMR (400 MHz, $CDCl_3$), δ (ppm); 8.38 (*d*, *J*=4.1 Hz, 1H), 8.19 (*d*, *J*=4.1 Hz, 1H), 7.89 (*m*, 3H), 7.51 (*m*, 2H), 4.17–4.08 (*m*, 4H),

1.72 (*d*, *J*=7.1 Hz, 4H), 1.45–1.16 (*m*, 20H), 0.89 (*t*, *J*=6.9 Hz, 6H). ^{13}C NMR (201 MHz, $CDCl_3$), δ (ppm): 192.37, 191.99, 167.50, 149.37, 144.35, 140.78, 134.40, 133.91, 131.87, 129.79, 124.62, 124.24, 122.90, 122.31, 45.03, 31.82, 29.73, 29.16, 27.06, 26.85, 22.65, 14.05. Anal. Calcd. for $C_{38}H_{41}F_1N_4O_2S_7$: C, 55.04; H, 4.98; N, 6.76; S, 27.07. Found: C, 56.68; H, 4.98; N, 6.74; S, 27.39.

Synthesis of **T-2FBT-T-ORH**: The synthetic procedure was performed under conditions analogous to those used for **T-BT-T-ORH**. 4,7-Dibromo-5,6-difluoro-2,1,3-benzothiadiazole (700 mg, 1.50 mmol) and B-T-ORH (198 mg, 0.600 mmol) were used as starting materials, together with $Pd_2(dba)_3$ (16.0 mg), P(*t*-Bu)$_3$·HBF$_4$ (10.0 mg), and THF (20 mL)/1 M K_3PO_4 (1.6 mL). After refluxing for 8.5 h under a nitrogen atmosphere, the product was isolated as a purple solid (158 mg, 31% yield). ^{1}H NMR (400 MHz, $CDCl_3$), δ (ppm): 8.38 (*d*, *J*=4.2 Hz, 1H), 7.93 (*s*, 1H), 7.59–7.50 (*m*, 1H), 4.19–4.06 (*m*, 2H), 1.73 (*s*, 2H), 1.30 (*t*, *J*= 20.5 Hz, 10H), 0.89 (*t*, *J*=6.9 Hz, 3H). ^{13}C NMR (201 MHz, $CDCl_3$), δ (ppm): 192.20, 167.50, 148.41, 141.29, 138.51, 133.78, 132.52, 124.29, 123.07, 111.92, 45.03, 31.80, 29.73, 29.15, 27.06, 26.84, 22.64, 14.05, 1.02. Anal. Calcd. for $C_{38}H_{40}F_2N_4O_2S_7$: C, 53.87; H, 4.76; N, 6.61; S, 26.49. Found: C, 53.93; H, 4.78; N, 6.47; S, 26.38.

Results and Discussion

Synthesis and Thermal Properties of the Small Molecules. A series of rod-shaped NFSMs with an A–D–A–D–A configuration were synthesized. All three molecules contain a T-BT-T core and RH end groups functionalized with alkyl substituents. For **T-1FBT-T-ORH** and **T-2FBT-T-ORH**, the BT core of **T-BT-T-ORH** was modified to include one or two fluorine atoms, respectively. Small molecules were prepared via Knoevenagel condensation followed by Suzuki coupling. The intermediate B-T-ORH was synthesized via a condensation reaction of ORH and 5-(4,4,5,5-tetramethyl-1,3,2-dioxaborolan-2-yl)thiophene-2-carboxaldehyde (B-T-CHO), and subsequent coupling with BT, 1FBT, or 2FBT afforded the corresponding products **T-BT-T-ORH**, **T-1FBT-T-ORH**, and **T-2FBT-T-ORH**. In addition, PBT7-Th is a low-bandgap polymer donor composed of benzo[1,2-*b*:4,5-*b*′]dithiophene and thieno[3,4-*b*]thiophene units. Its chemical structure is presented together with the synthetic route and molecular structures of the three NFSMs in Scheme 1. NMR characterization (^{1}H and ^{13}C) of the intermediates and the small molecules are available in the Supporting Information.

The thermal properties of the small molecules were investigated by thermogravimetric analysis (TGA) and DSC (Table 1). All compounds exhibited excellent thermal stability, with less than 5% weight loss up to 370 ℃ (Figure 1(a)). DSC analysis (Figure 1(b)) revealed that **T-BT-T-ORH** has distinctly lower melting and recrystallization temperatures (T_m and T_{cr}) than its fluorinated counterparts, **T-1FBT-T-ORH** and **T-2FBT-T-ORH**. Upon increasing the number of fluorine atoms, both the transition

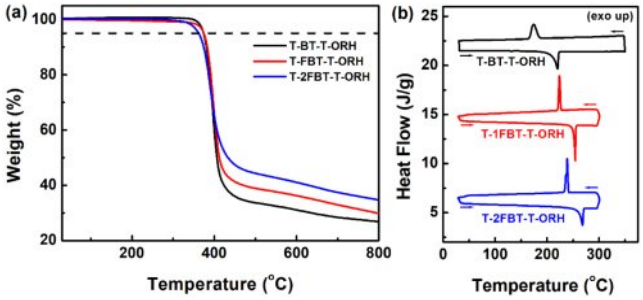

Figure 1. (a) TGA; (b) DSC curves of the small molecules.

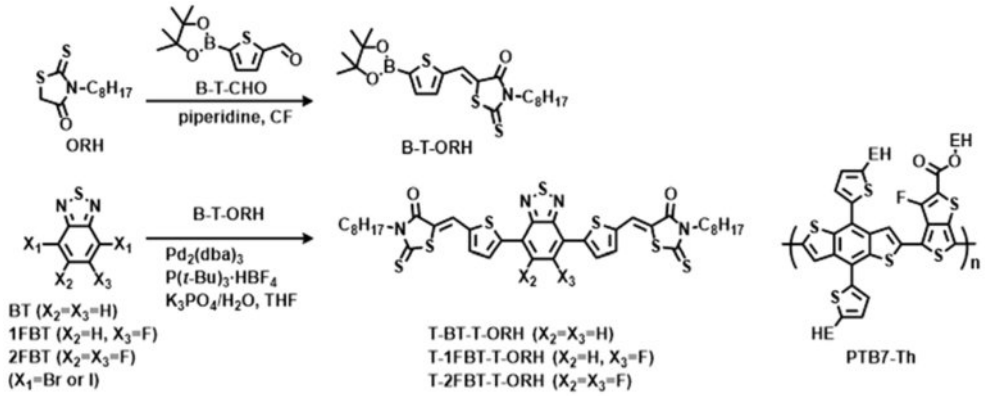

Scheme 1. Synthetic routes for **T-BT-T-ORH**, **T-1FBT-T-ORH**, and **T-2FBT-T-ORH**, along with the molecular structure of the PTB7-Th polymer donor.

Table 1. Thermal Properties of the Small Molecules

Small molecules	T_d (℃)[a]	T_m (℃)[b]	ΔH_m (J/g)[c]	T_{cr} (℃)[d]	ΔH_{cr} (J/g)[e]
T-BT-T-ORH	374	220	-43.5	174	39.2
T-1FBT-T-ORH	374	254	−71.7	223	68.2
T-2FBT-T-ORH	383	268	−73.8	239	75.0

[a]Temperature at which 5% weight loss is observed relative to the initial weight. [b]Temperature corresponding to the endothermic peak observed in the melting process. [c]Enthalpy change at T_m. [d]Temperature corresponding to the exothermic peak observed in the recrystallization process. [e]Enthalpy change at T_{cr}.

temperatures and enthalpy changes increased (Table 1), indicating that fluorine substitution strengthened the intermolecular interactions, thereby enhancing the crystallinity. The melting point progressively increased from 220 ℃ (**T-BT-T-ORH**) to 254 ℃ (**T-1FBT-T-ORH**) and 268 ℃ (**T-2FBT-T-ORH**). Similarly, the enthalpy changes increased from –43.5 J/g (**T-BT-T-ORH**) to –71.7 J/g (**T-1FBT-T-ORH**) and –73.8 J/g (**T-2FBT-T-ORH**). The recrystallization temperatures and corresponding enthalpy changes followed the same trend (Table 1), further confirming the enhanced crystallinity induced by fluorination.

Electrochemical and Optical Properties. The electrochemical properties of the synthesized molecules were systematically evaluated using CV (Figure 2). The highest occupied molecular orbital (HOMO) and the lowest unoccupied molecular orbital (LUMO) energy levels were estimated based on the empirical relations $E_{HOMO}=-(E_{onset,ox}-E_{1/2,Fc}+4.8)$ eV and $E_{LUMO}=-(E_{onset,red}-E_{1/2,Fc}+4.8)$ eV, where $E_{onset,ox}$ and $E_{onset,red}$ are oxidation and reduction onset potentials, respectively, and the ferrocene/ferrocenium (Fc/Fc^+) reference level is taken as 4.8 eV relative to the vacuum level.[26,27] Progressive fluorination of the BT unit induced a clear downshift of the frontier orbital energies. Specifically, the HOMO level decreased from −5.74 eV (**T-BT-T-ORH**) to −5.77 eV (**T-1FBT-T-ORH**) and further to −5.80 eV (**T-2FBT-T-ORH**). In contrast, the LUMO levels exhibited only minor changes, remaining at −3.58 eV for both **T-BT-T-ORH** and **T-1FBT-T-ORH** and slightly shifting to −3.60 eV for **T-2FBT-T-ORH**. Because the HOMO underwent more pronounced stabilization, the overall electrochemical bandgap widened upon fluorination. Importantly, the resulting energy alignment with the PTB7-Th polymer donor (Figure 2(b)) provided sufficient HOMO and LUMO offsets to enable efficient interfacial charge transfer, ensuring that exciton dissociation and charge separation proceeded effectively in the fabricated PSC devices. The electrochemical properties of the small molecules are listed in Table 2.

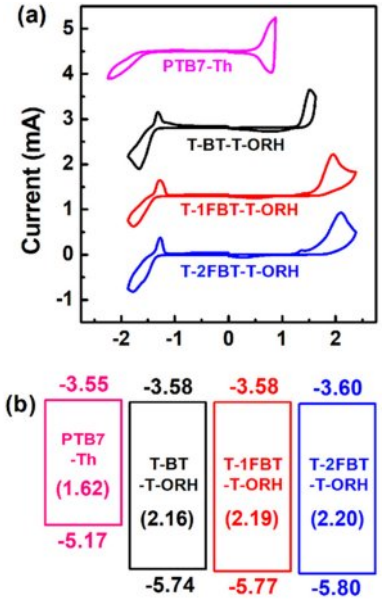

Figure 2. (a) CV curves; (b) energy diagrams of the small molecules and PTB7-Th.

The UV–vis absorption spectra of the small molecules are

Table 2. Electrochemical and Optical Properties of the Small Molecules

	E_{HOMO} (eV)[a]	E_{LUMO} (eV)[a]	$E_{g,CV}$ (eV)[a]	λ_{max} (nm)[b]		λ_{onset} (nm)[b]	$E_{g,opt}$ (eV)[c]
				Solution	Film		
T-BT-T-ORH	–5.74	–3.58	2.16	540	(585) 633	694	2.16
T-FBT-T-ORH	–5.77	–3.58	2.19	536	573 (622)	683	2.19
T-2FBT-T-ORH	–5.80	–3.60	2.20	520	556 (598)	656	2.20

[a]E_{HOMO}, E_{LUMO}, and $E_{g,CV}$ were obtained using CV. [b]λ_{max} and λ_{onset} represent the wavelengths of the absorption maximum and onset, respectively; shoulder peaks are shown in parentheses. [c]$E_{g,opt}$ represents the optical bandgap, estimated from λ_{onset} using the relation $E_{g,opt}=1240/\lambda_{onset}$ (eV).

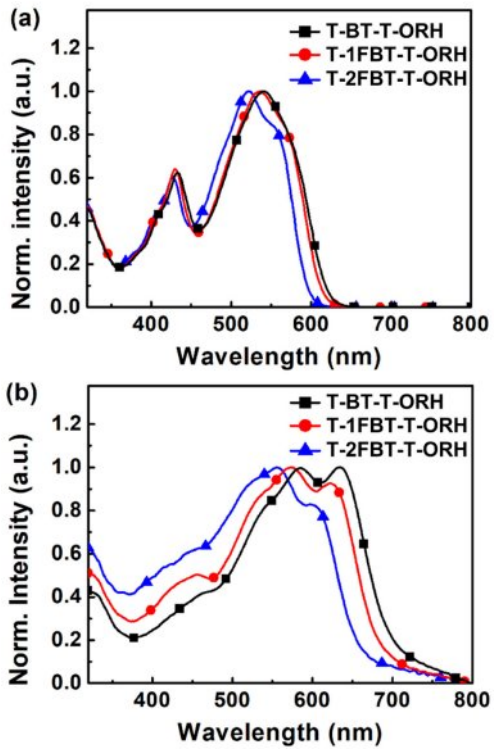

Figure 3. UV–vis absorption spectra of (a) the small molecules in solution; (b) films.

shown in Figure 3. The optical properties of the small molecules, including the absorption maxima (λ_{max}), absorption onset (λ_{onset}), and optical bandgap ($E_{g,opt}$), are listed in Table 2. As the number of fluorine substituents on the BT unit increased, the absorption bands gradually blue-shifted (Figure 3(a)). In chloroform solution, the λ_{max} of **T-BT-T-ORH**, **T-1FBT-T-ORH**, and **T-2FBT-T-ORH** were observed at 540 nm, 536 nm, and 520 nm, respectively. Similarly, the absorption spectra of the corresponding films exhibited progressive blue shifts with increasing fluorination (Figure 3(b)). The λ_{max} values of **T-BT-T-ORH**, **T-1FBT-T-ORH**, and **T-2FBT-T-ORH** films appeared at 633, 573, and 556 nm, respectively. This behavior can be rationalized by a decrease in the effective conjugation length within the molecular backbone, which arises from the introduction of fluorine atoms onto the BT ring. The incorporation of fluorine atoms not only alters the electronic distribution but also introduces steric hindrance owing to their relatively larger atomic radius compared to hydrogen. Such steric effects restrict the planarity of the conjugated backbone, thereby shortening the effective π-conjugation length and leading to higher-energy electronic transitions. These results are consistent with those of previous reports on fluorinated BT-based small molecules and polymers.[28-30] In these studies, fluorination was shown to stabilize the frontier orbitals, increase the bandgaps, and modulate the intermolecular interactions, thereby influencing charge transport. These results confirm that the controlled fluorination of BT units yields similar effects in our NFSM framework. Fluorine substitution directly influences conjugation and aggregation behavior in the solid state, ultimately widening the bandgap. Consistent with the trend of λ_{max} values, the λ_{onset} values were gradually blue-shifted with increasing fluorination, giving values of 694 nm (**T-BT-T-ORH**), 683 nm (**T-1FBT-T-ORH**), and 656 nm (**T-2FBT-T-ORH**). Consequently, the calculated $E_{g,opt}$ gradually increased from 1.79 eV (**T-BT-T-ORH**) to 1.81 eV (**T-1FBT-T-ORH**) and 1.90 eV (**T-2FBT-T-ORH**) upon the introduction of fluorine. This trend is consistent with the CV results. In addition, all films exhibited red-shifted and broadened absorption compared to the solution spectra, indicating *J*-type aggregation.

PSC Device Performances. The PSC devices were fabricated with an inverted configuration of indium tin oxide (ITO)/ZnO nanoparticles (NPs)/polyethylenimine ethoxylated (PEIE)/active layer/MoO_x/Ag. The active layer consisted of PTB7-Th and the acceptor in a weight ratio of 1:2, processed from chloroform solution. Post-annealing treatments of solvent vapor annealing (SVA) and thermal annealing (TA) were applied to optimize device performance. The optimized current density–voltage (*J–V*) curves and external quantum efficiency (EQE) spectra are shown in Figure 4, and the optimized photovoltaic performances are summarized in Table 3. Detailed fabrication procedures and additional device performance data are provided in the Supporting Information.

The as-cast device based on the non-fluorinated acceptor **T-BT-T-ORH** exhibited a PCE of 4.75%. Upon SVA, the device performance was further enhanced, achieving a maximum PCE of 6.92%. This improvement was accompanied by increases in both the short-circuit current density (J_{SC}) and fill factor (FF), reflecting an improved film morphology and balanced charge transport after annealing. In contrast, **T-1FBT-T-ORH** and **T-2FBT-T-ORH** delivered lower efficiencies in their as-cast states, with PCEs of 3.99% and 2.25%, respectively. The annealing treatment improved their performances to 5.89% and 2.47%, respectively, yet their efficiencies remained significantly lower than that of **T-BT-T-ORH**.

Importantly, all devices exhibited relatively high open-circuit voltages (V_{OC}), exceeding 0.90 V. These values are consistent with the CV results, in which the LUMO levels exhibited only minor differences, with values of −3.58 eV for both **T-BT-T-**

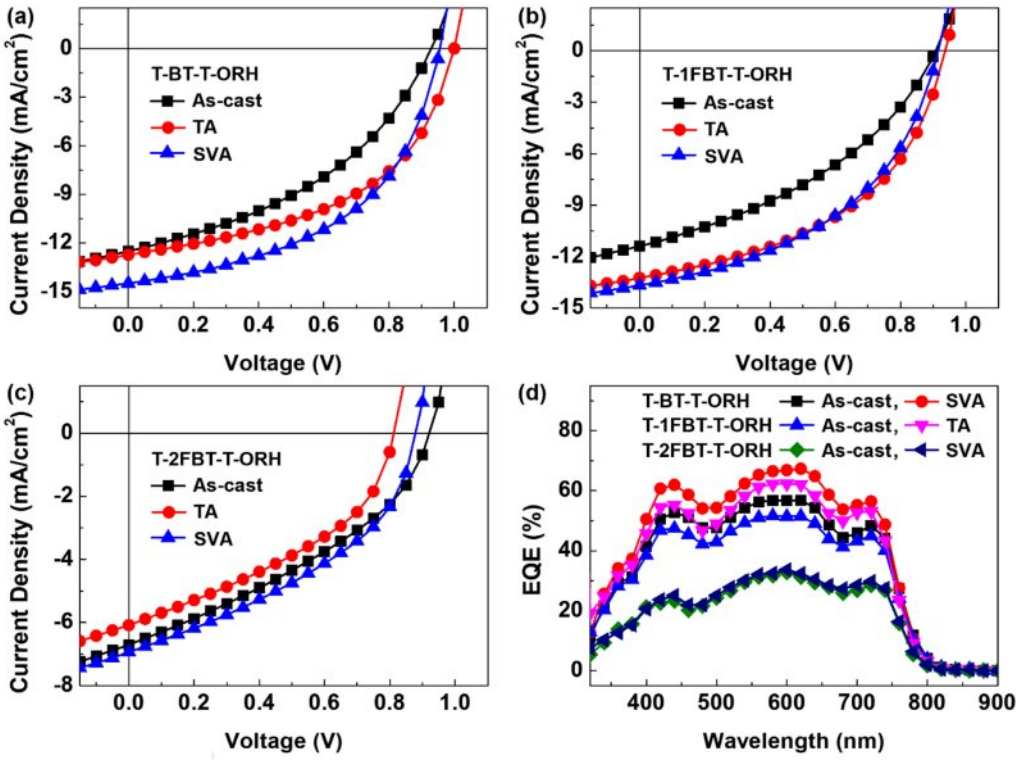

Figure 4. *J*–*V* curves based on (a) **T-BT-T-ORH**; (b) **T-1FBT-T-ORH**; (c) **T-2FBT-T-ORH**; (d) EQE spectra of PTB7-Th:acceptor devices.

Table 3. Optimized Device Performance of PTB7-Th:Acceptor Devices

Acceptors	Annealing	V_{OC} (V)	J_{SC} (mA/cm^2)	FF (%)	PCE (%)
T-BT-T-ORH	As-cast	0.93	12.51	41	4.75
	SVA	0.96	14.49	50	6.92
T-1FBT-T-ORH	As-cast	0.91	11.41	39	3.99
	TA	0.94	13.25	47	5.89
T-2FBT-T-ORH	As-cast	0.92	6.70	36	2.25
	SVA	0.88	6.93	41	2.47

ORH and **T-1FBT-T-ORH** and a slight shift to −3.60 eV for **T-2FBT-T-ORH**. Therefore, the V_{OC} values did not vary significantly among the devices, except that the annealed **T-2FBT-T-ORH** device showed a slightly reduced V_{OC} compared with its as-cast counterpart. To further evaluate the energetics of the devices, the energy loss (E_{loss}=$E_{g,opt}$–qV_{OC}) was determined using the lower optical bandgap between donor and acceptor component ($E_{g,opt}$=1.58 eV).[31]

For most devices, with V_{OC} values above 0.91 V, the corresponding E_{loss} values were maintained below 0.67 eV, indicating low energy loss favorable for device performance. In contrast, the lower V_{OC} of the annealed **T-2FBT-T-ORH** device (0.88 V) is explained by its relatively large E_{loss} of 0.70 eV. Overall, all devices maintained relatively high V_{OC} values and low energy losses, which are advantageous for achieving high device performance.

Moreover, the annealing treatment improved both J_{SC} and FF, leading to enhanced device performance in all devices. For example, the J_{SC} of the **T-BT-T-ORH**-based device increased from 12.51 to 14.49 mA cm^{-1} by annealing treatment. Similar improvements were observed for the fluorinated analogs, with **T-1FBT-T-ORH** increasing from 11.41 to 13.25 mA cm^{-1}, and **T-2FBT-T-ORH** from 6.70 to 6.93 mA cm^{-1}. These enhancements reflect improved film morphology and more balanced

charge transport upon annealing. The EQE spectra (Figure 4(b)) further confirm this trend, showing increased photocurrent responses over the spectral range of 400–800 nm after treatment. However, the introduction of fluorine substituents induced stronger intermolecular aggregation, as evidenced by the broadened absorption spectra and higher crystallinity observed in the UV–vis absorption and DSC measurements. While such aggregation can be beneficial for charge transport in some systems, it leads to poor solubility in chloroform solutions and an unfavorable blend morphology with PTB7-Th in this case, showing suppressed J_{SC} and FF values relative to the non-fluorinated analogs.

Overall, these results highlight the trade-off introduced by fluorination; although fluorination stabilizes the frontier orbitals and enhances molecular crystallinity, it simultaneously compromises solubility and blend miscibility with PTB7-Th. Consequently, the photovoltaic efficiency of the fluorinated NFSMs was inferior to their non-fluorinated counterpart. Nevertheless, these findings suggest that careful control of fluorination can enable a better balance between electronic stabilization and favorable film morphology, offering valuable design guidelines for future high-performance PSCs.

Conclusion

In this study, we synthesized and characterized a series of rod-shaped NFSM acceptors, **T-BT-T-ORH**, **T-1FBT-T-ORH**, and **T-2FBT-T-ORH**, by systematically introducing 0, 1, and 2 F atoms into the BT unit to investigate their impact on PSC performance. When fabricated with PTB7-Th as the polymer donor, the non-fluorinated **T-BT-T-ORH** achieved the highest PCE of 6.92% after SVA treatment. In contrast, **T-1FBT-T-ORH** and **T-2FBT-T-ORH** exhibited lower efficiencies of 5.89% and 2.47%, respectively. DSC analysis confirmed that fluorination successfully strengthened intermolecular interactions, as evidenced by the significant increase in melting temperatures and enthalpy changes for the fluorinated acceptors. In this work, such enhanced crystallinity led to excessive intermolecular aggregation and poor solubility in chloroform, resulting in an unfavorable blend morphology with the PTB7-Th. Consequently, the J_{SC} and FF values were effectively suppressed relative to the non-fluorinated analog. These findings demonstrate that while fluorination is a powerful tool for stabilizing frontier orbital levels and reinforcing molecular packing, it introduces a critical trade-off between electronic stabilization and film-forming properties. Therefore, precise control over the degree of fluorination is essential to balance molecular crystallinity with optimal blend miscibility, providing valuable design guidelines for high-performance NFSM-based PSCs.

Acknowledgements: This work was supported by the 2025 Research Fund of the University of Seoul.

Conflict of Interest: The authors declare that there is no conflict of interest.

Supporting information: Information is available regarding the experimental procedure including ^{1}H and ^{13}C NMR spectroscopy of the intermediates and the small molecules and the detailed device performances are listed in Supporting The materials are available *via* the Internet at http://journal.polymer-korea.or.kr.

References

1. Shen, Y. F.; Zhang, H.; Zhang, J.; Tian, C.; Shi, Y.; Qiu, D.; Zhang, Z.; Lu, K.; Wei, Z. In Situ Absorption Characterization Guided Slot-Die-Coated High-Performance Large-Area Flexible Organic Solar Cells and Modules. *Adv. Mater.* **2023**, 35, 2209030.
2. Zhang, G.; Lin, F. R.; Qi, F.; Heumüller, T.; Distler, A.; Egelhaaf, H.-J.; Li, N.; Chow, P. C. Y.; Brabec, C. J.; Jen, A. K. Y.; Yip, H.-L. Renewed Prospects for Organic Photovoltaics. *Chemical Reviews* **2022**, 122, 14180-14274.
3. Liu, B.; Sandberg, O. J.; Qin, J.; Liu, Y.; Wilken, S.; Wu, N.; Yu, X.; Fang, J.; Li, Z.; Huang, R.; Zha, W.; Luo, Q.; Tan, H.; Österbacka, R.; Ma, C.-Q. Inverted Organic Solar Cells with an In Situ-derived SiO_xNy Passivation Layer and Power Conversion Efficiency Exceeding 18%. *Nat. Photon.* **2025**, 19, 195-203.
4. Jung, W.; Hong, S.; Moon, S. M.; Son, S. Y. Synthesis of Photoactive Layer Materials in Organic Photovoltaics: an Asymmetric Molecular Approach. *Polym. Korea* **2024**, 48, 594-602.
5. Ayuningtias, L.; Ma, J. Y.; Kim, Y.-J.; Kim, Y.-H. Synthesis and Characterization of Diketopyrrolopyrrole-based Conjugated Polymer with Biphenyl for Organic Photovoltaic Cells. *Bull. Kor. Chem. Soc.* **2025**, 46, 754-760.
6. Zhang, Y.; Zhang, Y.; Liu, X.; Geng, Z.; Wang, H.; Xu, Z.; Miao, Z.; Liang, Q.; Liu, J. Controlling the Third Component Distribution Toward High-Efficient Ternary Organic Solar Cells. *Adv. Energ. Mater.* **2025**, 15, 2406136.
7. Lee, S.; Kwak, S. L.; Park, H. J.; Hwang, D.-H. Pyridoquinolinedione as a New Building Block for Semiconducting Polymer Donors in Organic Solar Cells. *Polym. Korea* **2025**, 49, 556-563.
8. Jun, M.; Seo, J.-Y. Study on Thin Film Encapsulation Coating for Long-term Stable Organic Solar Cells. *Polym. Korea* **2023**, 47, 87-91.
9. Lin, Y.; Wang, J.; Zhang, Z. G.; Bai, H.; Li, Y.; Zhu, D.; Zhan, X. An Electron Acceptor Challenging Fullerenes for Efficient Polymer Solar Cells. *Adv. Mater.* **2015**, 27, 1170.
10. Yuan, J.; Zhang, Y.; Zhou, L.; Zhang, G.; Yip, H. L.; Lau, T. K.;

Lu, X.; Zhu, C.; Peng, H.; Johnson, P. A. Single-Junction Organic Solar Cell with over 15% Efficiency Using Fused-Ring Acceptor with Electron-Deficient Core. *Joule* **2019**, 3, 1140.
11. Jiang, Y.; Sun, S.; Xu, R.; Liu, F.; Miao, X.; Ran, G.; Liu, K.; Yi, Y.; Zhang, W.; Zhu, X. Non-fullerene Acceptor with Asymmetric Structure and Phenyl-substituted Alkyl Side Chain for 20.2% Efficiency Organic Solar Cells. *Nat. Energy* **2024**, 9, 975.
12. Jiang, Y.; Liu, K.; Liu, F.; Ran, G.; Wang, M.; Zhang, T.; Xu, R.; Liu, H.; Zhang, W.; Wei, Z.; Cui, Y.; Lu, X.; Hou, J.; Zhu, X. 20.6% Efficiency Organic Solar Cells Enabled by Incorporating a Lower Bandgap Guest Nonfullerene Acceptor Without Open-Circuit Voltage Loss. *Adv. Mater.* **2025**, 37, 2500282.
13. Wang, S.; Wang, S.; Wang, J.; Yu, N.; Qiao, J.; Xie, X.; Li, C.; Abbasi, M. S.; Ding, R.; Zhang, X.; Han, Y.; Lu, G.; Zhang, J.; Hao X.; Tang, Z.; Cai, Y.; Huang, H. Achieving 20% Efficiency in Organic Solar Cells Through Conformationally Locked Solid Additives. *Adv. Energ. Materi.* **2025**, 2405205.
14. Li, C.; Song, J.; Lai, H.; Zhang, H.; Zhou, R.; Xu, J.; Huang, H.; Liu, L.; Gao, J.; Li, Y.; Jee, M. H.; Zheng, Z.; Liu, S.; Yan, J.; Chen, X.-K.; Tang, Z.; Zhang, C.; Woo, H. Y.; He, F.; Gao, F.; Yan, H.; Sun, Y. Non-Fullerene Acceptors with High Crystallinity and Photoluminescence Quantum Yield Enable >20% Efficiency Organic Solar Cells. *Nat. Mater.* **2025**, 24, 433-443.
15. Chen, C.; Wang, L.; Xia, W.; Qiu, K.; Guo, C.; Gan, Z.; Zhou, J.; Sun, Y.; Liu, D.; Li, W.; Wang, T. Molecular Interaction Induced Dual Fibrils Towards Organic Solar Cells with Certified Efficiency Over 20%. *Nat. Commun.* **2024**, 15, 6865.
16. Wang, Y.; Yang, M.; Chen, Z.; Zhong, J.; Zhao, F.; Wei, W.; Yuan, X.; Zhang, W.; Ma, Z.; He, Z.; Liu, Z.; Huang, F.; Cao, Y.; Duan, C. Fully Non-fused Electron Acceptor Solar Cells with 18% Efficiency *via* a Synergistic Peripheral Substituent Strategy. *Nat. Commun.* **2025**, 16, 5449.
17. Zhang, W.; Zhao, K.; Zhang, N.; Dong, Q.; Shen, S.; Lu, H.; Hu, B.; Zhao, F.; Yuan, S.; Lu, G.; Chen, Y.; Ma, Z.; Bo, Z.; Song, J. Backbone Twisting and Terminal Overlapping *via* Π-bridge Engineering for Highly Efficient Non-fused Ring Electron Acceptors with Balanced J_{SC}-V_{OC}. *Adv. Funct. Mater.* **2025**, 35, 2423242.
18. Lee, M.; Hwang, E.; Kim, T.; Kwon, T.-H. Advancements in Non-fullerene Acceptors for Organic Solar Cells: Brief Review of Research Trends. *Bull. Kor. Chem. Soc.* **2024**, 45, 664-674.
19. Shao, J.; Li, M.; Chen, G.; Fang, Y.; Young Jeong, S.; Ke, Y.; Yi, X.; Young Woo, H.; Huang, B. Developing a Fluorinated Benzothiadiazole-Based Polymer Donor as Guest to Construct High-Performance Ternary Solar Cells. *ChemSusChem* **2025**, 18, e202402226.
20. Wang, S.; Pan, C.; Li, W.; Sun, H.; Zhang, J.; Dong, L.; Zhuang, W.; Huang, W. Modulating Optoelectronic Performance Through Strategic Chlorine Substitution in Diketopyrrolopyrrole-Based Conjugated Polymers. *Langmuir* **2025**, 41, 15364-15371.
21. Rodríguez-Seco, C.; Biswas, S.; Sharma, G. D.; Vidal-Ferran, A.; Palomares, E. Benzothiadiazole Substituted Semiconductor Molecules for Organic Solar Cells: The Effect of the Solvent Annealing Over the Thin Film Hole Mobility Values. *J. Phys. Chem. C* **2018**, 122, 13782-13789.
22. Yang, L.; Gu, W.; Yang, Y.; Hong, L.; Zhang, X.; Xiao, Y.; Wu, X.; Peng, A.; Huang, H. A Highly Planar Nonfullerene Acceptor with Multiple Noncovalent Conformational Locks for Efficient Organic Solar Cells. *Small Methods* **2018**, 2, 1700330.
23. Kamimura, S.; Saito, M.; Teshima, Y.; Yamanaka, K.; Ichikawa, H.; Sugie, A.; Yoshida, H.; Jeon, J.; Kim, H. D.; Ohkita, H.; Mikie, T.; Osaka, I. Manipulating the Functionality and Structures of π-Conjugated Polymers Utilizing Intramolecular Noncovalent Interactions Towards Efficient Organic Photovoltaics. *Chem. Sci.* **2024**, 15, 6349-6362.
24. Saito, M.; Fukuhara, T.; Kamimura, S.; Ichikawa, H.; Yoshida, H.; Koganezawa, T.; Ie, Y.; Tamai, Y.; Kim, H. D.; Ohkita, H.; Osaka, I. Impact of Noncovalent Sulfur–Fluorine Interaction Position on Properties, Structures, and Photovoltaic Performance in Naphthobisthiadiazole-Based Semiconducting Polymers. *Adv. Energ. Mater.* **2020**, 10, 1903278.
25. Chen, H.; Liang, H.; Guo, Z.; Zhu, Y.; Zhang, Z.; Li, Z.; Cao, X.; Wang, H.; Feng, W.; Zou, Y.; Meng, L.; Xu, X.; Kan, B.; Li, C.; Yao, Z. Central Unit Fluorination of Non-Fullerene Acceptors Enables Highly Efficient Organic Solar Cells with Over 18% Efficiency. *Angew. Chem. Int. Ed.* **2022**, 61, e202209580.
26. Kwon, O.; Jo, J.; Walker, B.; Bazan, G. C.; Seo, J. H. Pendant Group Effects on the Optical and Electrical Properties of Carbazole-diketopyrrolopyrrole Copolymers. *J. Mater. Chem. A* **2013**, 1, 7118-7124.
27. Zhang, T.; Zhao, X.; Yang, D.; Tian, Y.; Yang, X. Ternary Organic Solar Cells with >11% Efficiency Incorporating Thick Photoactive Layer and Nonfullerene Small Molecule Acceptor. *Adv. Energ. Mater.* **2018**, 8, 1701691.
28. Liu, X.; Sun, Y.; Hsu, B. B. Y.; Lorbach, A.; Qi, L.; Heeger, A. J.; Bazan, G. C. Design and Properties of Intermediate-Sized Narrow Band-Gap Conjugated Molecules Relevant to Solution-Processed Organic Solar Cells. *J. Am. Chem. Soc.* **2014**, 136, 5697-5708.
29. Li, Y.; Zou, J.; Yip, H.-L.; Li, C.-Z.; Zhang, Y.; Chueh, C.-C.; Intemann, J.; Xu, Y.; Liang, P.-W.; Chen, Y.; Jen. A. K. Y. Side-Chain Effect on Cyclopentadithiophene /Fluorobenzothiadiazole-Based Low Band Gap Polymers and Their Applications for Polymer Solar Cells. *Macromolecules* **2013**, 46, 5497-5503.
30. Neo, W. T.; Ong, K. H.; Lin, T. T.; Chua, S.-J.; Xu, J. Effects of Fluorination on the Electrochromic Performance of Benzothiadiazole-based Donor-acceptor Copolymers. *J. Mater. Chem. C* **2015**, 3, 5589-5597.
31. Lee, T.; Eom, Y.; Song, C. E.; Jung, I. H.; Kim, D.; Lee, S. K.; Shin, W. S.; Lim, E. Simple Bithiophene–Rhodanine-Based Small Molecule Acceptor for Use in Additive-Free Nonfullerene OPVs with Low Energy Loss of 0.51 eV. *Adv. Energ. Mater.* **2019**, 9, 1804021.